NASA Technical Memorandum 85958

A Computational Method for Viscous Incompressible Flows

Dochan Kwak and James L.C. Chang

May 1984

National Aeronautics and
Space Administration

NASA Technical Memorandum 85958

A Computational Method for Viscous Imcompressible Flows

Dochan Kwak, Ames Research Center, Moffett Field, California

James L. C. Chang, Rocketdyne Division, Rockwell International, Canoga Park, California

National Aeronautics and
Space Administration

Ames Research Center
Moffett Field, California 94035

A COMPUTATIONAL METHOD FOR VISCOUS INCOMPRESSIBLE FLOWS

Dochan Kwak
NASA Ames Research Center
Moffett Field, California

James L.C. Chang
Rocketdyne Division, Rockwell International
Canoga Park, California

Abstract

An implicit, finite-difference procedure for numerically solving viscous incompressible flows is presented. The pressure-field solution is based on the pseudocompressibility method in which a time-derivative pressure term is introduced into the mass-conservation equation to form a set of hyperbolic equations. The pressure-wave propagation and the spreading of the viscous effect is investigated using simple test problems. Computed results for external and internal flows are presented to verify the present method which has proved to be very robust in simulating incompressible flows.

I. Introduction

Incompressible flow phenomena are frequently encountered in many engineering applications, especially, in hydrodynamics and in certain classes of aerodynamic problems such as dynamic stall and low-speed wind-tunnel test problems. For most two-dimensional flow simulations, computer time and memory requirements are not major limiting factors, and various numerical techniques have been implemented quite successfully. For example, a stream function-vorticity formulation is frequently used for solving two-dimensional, viscous, incompressible flow problems (for example, see ref. 1). This approach conveniently eliminates the pressure terms. The three-dimensional extension of this method, however, is not straightforward. Various other three-dimensional viscous-flow solvers have been developed, mainly, for compressible flow (for example, see refs. 2-5). Implementing these procedures for simulating viscous incompressible flows is not efficient and is generally not recommended. Therefore, it is desirable to develop an efficient computational method for solving viscous incompressible flows. For convenience in applying the method to three-dimensional problems, primitive variables, namely, the pressure and velocities, are used in the present work.

One of the major difficulties in solving incompressible flows that use primitive variables is caused by the presence of the pressure term which is used as a mapping parameter to obtain a divergence-free velocity field. One method of solving for pressure is the Poissons equation approach developed by Harlow and Welch [6], which has been used frequently, mostly in conjunction with explicit methods. The usual computational procedure is to choose the pressure field such that continuity is satisfied at the next time-level, so that the new flow field will be divergence-free. This procedure normally requires a relaxation scheme iterating on pressure until the divergence-free condition is reasonably satisfied. Because this approach can be very time consuming, the computing time required for simulating three-dimensional flows has been prohibitively large. To accelerate the pressure-field solution and alleviate the drawback associated with the Poissons equation approach, Chorin [7] proposed the use of artificial compressibility in solving the continuity equation. A similar method was adopted by Steger and Kutler [8] using an implicit approximate-factorization scheme due to Beam and Warming [9]. To implement the implicit time-differencing, a hyperbolic time-dependent system of equations is fabricated by adding a time-derivative of the pressure term to the mass-conservation equation. These hyperbolic equations possess characteristics that are not present in the usual Poisson's equation for pressure. This approach has been applied to simulate laminar, incompressible flow within liquid-filled shells [10]. Based on this procedure, a pseudocompressible method has been developed for solving three-dimensional, viscous, incompressible flow problems cast in generalized curvilinear coordinates [11,12]. The purpose of the present paper is to show salient features of the pseudocompressible approach using numerical experiments.

The method is described in section II, the numerical algorithm is explained in section III, and computational experiments are presented in section IV to show the physical characteristics of the present method.

II. Description of the Method

Incompressible Navier-Stokes Equations

Unsteady, three-dimensional, viscous, incompressible flow with constant density is governed by the following Navier-Stokes equations, written in tensor notation:

$$\frac{\partial u_i}{\partial x_i} = 0 \tag{1a}$$

$$\frac{\partial u_i}{\partial t} + \frac{\partial u_i u_j}{\partial x_j} = -\frac{\partial p}{\partial x_i} + \frac{\partial \tau_{ij}}{\partial x_j} \tag{1b}$$

Here, t is time; x_i are the Cartesian coordinates; u_i are

corresponding velocity components; p is the pressure; and τ_{ij} is the viscous stress tensor. The viscous stress tensor can be written in the following form:

$$\tau_{ij} = 2\nu S_{ij} - R_{ij} \tag{1c}$$

The strain rate tensor is defined by

$$S_{ij} = \frac{1}{2}\left(\frac{\partial u_i}{\partial x_j} + \frac{\partial u_j}{\partial x_i}\right) \tag{1d}$$

Here, R_{ij} is the Reynolds stresses, and ν is the coefficient of viscosity. Since the expression for the Reynolds-stress terms depends on the turbulence closure model used, the accuracy of the turbulent flow problems will naturally depend on the level of the model and on experimental input used for calibrating the model. Because economy is still an overriding factor in many engineering applications, turbulence is often simulated by an algebraic eddy-viscosity model, using a constitutive equation involving a " mixing length" as a measure of the turbulence length scale. In the present study, however, only laminar flows are considered in order to remove any uncertainties involving the turbulence modeling.

The equations are written in dimensionless form with

$$\begin{aligned} \tilde{u}_i &= \frac{u_i}{u_{ref}}, \quad \tilde{p} = \frac{p - p_{ref}}{\rho u_{ref}^2}, \quad \tilde{\tau}_{ij} = \frac{\tau_{ij}}{\rho u_{ref}^2}, \\ \tilde{x}_i &= \frac{x_i}{x_{ref}}, \quad \tilde{t} = \frac{t u_{ref}}{x_{ref}}, \\ \tilde{\nu} &= Re^{-1} = \frac{\nu}{x_{ref} u_{ref}}, \quad \tilde{\beta} = \frac{\beta}{u_{ref}^2} \end{aligned} \tag{1e}$$

The subscript ref denotes reference quantities, and for convenience the tildes are dropped from the equations.

Pseudocompressible Formulation

The system of equations given above is not as readily solvable by a fast alternating-direction-implicit (ADI) scheme as the unsteady compressible Navier-Stokes equations which are hyperbolic. This difficulty can be alleviated by modifying the continuity equation as follows (see refs. 11,12):

$$\frac{1}{\beta}\frac{\partial p}{\partial t} + \frac{\partial u_i}{\partial x_i} = 0 \tag{1f}$$

The parameter $1/\beta$ is the pseudocompressibility. As the solution converges to a steady state, the pseudocompressibility effect approaches zero yielding the incompressible form of the equations.

For time-dependent problems, a pressure iteration term is added to the right-hand side of equation (1f) as follows:

$$\frac{1}{\beta}\frac{\partial p}{\partial t} + \frac{\partial u_i}{\partial x_i} = \frac{1}{\beta}\frac{\partial p^*}{\partial t} \tag{1g}$$

Here, p^* is the value of p at the previous iteration. The pressure must be iterated until the divergence-free velocity field is obtained within the desired numerical accuracy.

The present method is primarily designed for obtaining steady-state solutions efficiently, and our interest here is limited to the development of the steady-state algorithm.

Physical Meaning of the Pseudocompressibility

The system of equations governing the motion of an incompressible flow is elliptic. In the elliptic formulation, pressure waves propagate with infinite speed. However, the system of modified equations given by equations (1b) and (1f) is hyperbolic. Thus, in the present formulation, waves of finite speed are introduced. The magnitude of the wave speed depends on β. In viscous flows, the behavior of the boundary layer is very sensitive to the local presure gradient, especially when the boundary layer is separated. For example, if the local pressure gradient oscillates owing to the traveling pressure waves of finite speed that are generated numerically, the location of the flow separation may fluctuate accordingly. This unsteady behavior of the separation will feed back to the pressure field, making it difficult to obtain steady-state solutions. Therefore, the following aspects are of prime importance for the success of the present method: (1) how the introduced waves of finite speed must propagate relative to the viscous effect to simulate the incompressible flows, (2) how to choose the value of β to achieve computational efficiency, and (3) how to guarantee the incompressibility and the accuracy of the solution. These aspects are analyzed in previous papers [11,12], and numerical experiments are presented here to demonstrate the characteristics of the present procedure.

Lower Bound of β

Equation (1f) shows that $\partial u_i/\partial x_i$ approaches zero when $\beta >> 1$. However, since the magnitude of β controls the speed of the pressure wave, it plays a very important role in determining convergence speed, accuracy, and stability. By simplifying the governing equation to a one-dimensional linearized form, propagation characteristics of the pressure wave can be studied [12]. If the velocity in the primary flow direction is represented by u, the pseudosound speed c for this system of equations is

$$c = \sqrt{u^2 + \beta} \tag{2}$$

The dimensionless time scale, τ_L (i.e., the time it takes for the upstream propagating wave to travel a distance L) becomes

$$\tau_L = \frac{L/x_{ref}}{c - u} \tag{3a}$$

The spreading of the viscous effect can be represented by the boundary-layer growth rate. Therefore, for laminar flows, the time required for the viscous effect to spread over a thickness δ is approximately given by

$$\tau_\delta \simeq \frac{Re}{4}\left(\frac{\delta}{x_{ref}}\right)^2 \tag{3b}$$

To recover the incompressible phenomena, the physics requires that the pressure wave propagates much faster than the spreading of vorticity, namely,

$$\tau_L << \tau_\delta \tag{4}$$

From this, a criterion for the lower bound of β is obtained as follows:

$$\beta >> [1+\frac{4}{Re}\left(\frac{x_{ref}}{x_\delta}\right)^2\left(\frac{x_L}{x_{ref}}\right)]^2-1 \tag{5a}$$

When this requirement is not satisfied, the numerical procedure can diverge or the rate of convergence becomes so slow that it is practically impossible to obtain a converged solution. A similar analysis leads to a criterion for turbulent flows as follows:

$$\beta >> [1+\frac{1}{Re_t}\left(\frac{x_{ref}}{x_\delta}\right)^2\left(\frac{x_L}{x_{ref}}\right)]^2-1 \tag{5b}$$

Equations (5a) and (5b) set the lower bound of β. The upper bound will be discussed in a later section.

One of the other aspects to be considered is the total number of iterations required for the wave to travel downstream and back upstream, which is a total distance of $2L$. Recalling that the downstream and upstream traveling waves propagate with speed $(c+u)$ and $(c-u)$ respectively, the total time required for one round trip, τ_1, can be written as

$$\tau_1 = \frac{\sqrt{u^2+\beta}}{\beta}2L \tag{6a}$$

If a constant time-step is used throughout the computation, the total number of iterations N_1 for one round trip is

$$N_1 = \frac{\tau_1}{\Delta\tau} \tag{6b}$$

where $\Delta\tau$ is the increment of dimensionless time. For convergence, enough computing time τ has to elapse to permit the wave to make at least one round trip. This aspect will be demonstrated later using test problems.

III. Numerical Algorithm

Difference Equations

To accommodate fully three-dimensional geometries, the following generalized independent variables are introduced which transform the physical coordinates into general curvilinear coordinates:

$$\begin{aligned}\tau &= t\\ \xi &= \xi(x,y,z,t)\\ \eta &= \eta(x,y,z,t)\\ \varsigma &= \varsigma(x,y,z,t)\end{aligned} \tag{7}$$

Applying this transformation to the governing equations (1b) and (1f), and combining trapezoidal-rule time-differencing and the difference form of the transformed governing equations, the following equation in delta-form is obtained:

$$\begin{aligned}&\left\{I+\frac{h}{2}J^{n+1}[\delta_\xi(\hat{A}_1{}^n-\Gamma_1)+\delta_\eta(\hat{A}_2{}^n-\Gamma_2)\right.\\ &\qquad\left.+\delta_\varsigma(\hat{A}_3{}^n-\Gamma_3)]\right\}(\hat{Q}^{n+1}-\hat{Q}^n)\\ &=(I-I_m)(p^*-p^n)-(I-\frac{J^{n+1}}{J^n})\hat{Q}^n\\ &\quad -hJ^{n+1}(\delta_\xi\hat{E}_1{}^n+\delta_\eta\hat{E}_2{}^n+\delta_\varsigma\hat{E}_3{}^n)\\ &\quad +hJ^{n+1}(\delta_\xi\Gamma_1+\delta_\eta\Gamma_2+\delta_\varsigma\Gamma_3)\hat{Q}^n\end{aligned} \tag{8}$$

where

$J = Jacobian\ \ of\ \ the\ \ transformation$

$$\hat{Q}=\begin{bmatrix}p\\u\\v\\w\end{bmatrix},\quad I_m=\begin{bmatrix}0&0&0&0\\0&1&0&0\\0&0&1&0\\0&0&0&1\end{bmatrix}$$

$$\hat{E}_i{}^n=\frac{1}{J}\begin{bmatrix}\beta u_i+L_0(p-\beta)\\ uU_i+L_1p\\ vU_i+L_2p\\ wU_i+L_3p\end{bmatrix} \tag{9}$$

$$\hat{A}_i{}^n=\begin{bmatrix}L_0 & (L_1\beta) & (L_2\beta) & (L_3\beta)\\ L_1 & (U_i+L_1u) & L_2u & L_3u\\ L_2 & L_1v & (U_i+L_2v) & L_3v\\ L_3 & L_1w & L_2w & (U_i+L_3w)\end{bmatrix}$$

Here, the contravariant velocities, U_i without metric normalization, are defined as

$$U_i = L_0+L_1u+L_2v+L_3w \tag{10}$$

where

$L_0=(\xi_i)_t,\quad L_1=(\xi_i)_x,\quad L_2=(\xi_i)_y,\quad L_3=(\xi_i)_z$

$\xi_i=\xi,\eta,\ \ or\ \ \varsigma\ \ for\ \ i=1,2,\ \ or\ \ 3,\ \ respectively$

$\delta_\xi = finite\ \ difference\ \ form\ \ of\ \ \frac{\partial}{\partial\xi},etc.$

$h=\Delta\tau=time-step$

The superscript n denotes the n_{th} time-step, and the viscous terms are given as

$$\Gamma_i=\frac{\nu}{J}(\nabla\xi_i\nabla\xi_jI_m\frac{\partial}{\partial\xi_j}) \tag{11}$$

Approximate Factorization

The full viscous terms in Eq. (11) produce nontridiagonal elements in the left-hand side of equation (8). Therefore, to implement an approximate-factorization scheme, only orthogonal terms are kept on the left-hand side. For steady-state solutions, this can be done since the left-hand side approaches zero as a steady state is approached. For a time-accurate solution, this approximation procedure needs to be further investigated when a nonorthogonal grid is used. For the right-hand side, the full viscous terms may be included. Presently, a nearly orthogonal grid is used, and the viscous terms are further simplified to

$$\Gamma_i=\frac{\nu}{J}(\nabla\xi_i\cdot\nabla\xi_i)I_m\frac{\partial}{\partial\xi_i}=\gamma_iI_m\frac{\partial}{\partial\xi_i} \tag{12}$$

After adding smoothing terms to stabilize the computation, the approximate-factored form of the governing equation becomes

$$[I+\frac{h}{2}J^{n+1}\delta_\xi(\hat{A}_1{}^n-\gamma_1 I_m\delta_\xi)+\epsilon_i\nabla_\xi\Delta_\xi]\cdot$$
$$[I+\frac{h}{2}J^{n+1}\delta_\eta(\hat{A}_2{}^n-\gamma_2 I_m\delta_\eta)+\epsilon_i\nabla_\eta\Delta_\eta]\cdot$$
$$[I+\frac{h}{2}J^{n+1}\delta_\zeta(\hat{A}_3{}^n-\gamma_3 I_m\delta_\zeta)+\epsilon_i\nabla_\zeta\Delta_\zeta](\hat{Q}^{n+1}-\hat{Q}^n)$$
$$=[RHS\quad(7)]-\epsilon_e[(\nabla_\xi\Delta_\xi)^2+(\nabla_\eta\Delta_\eta)^2+(\nabla_\zeta\Delta_\zeta)^2]\hat{Q}^n \tag{13}$$

where ϵ_i and ϵ_e are implicit and explicit smoothing terms, and

$$h=\Delta\tau=time-step$$
$$\nabla_\xi\hat{Q}=\hat{Q}_j-\hat{Q}_{j-1},\quad \Delta_\eta\hat{Q}=\hat{Q}_{k+1}-\hat{Q}_k$$
$$\delta_\zeta\hat{Q}=(\hat{Q}_{l+1}-\hat{Q}_{l-1})/(2\Delta\zeta)$$
$$\delta_\eta\gamma\delta_\eta\hat{Q}=[(\gamma_{k+1}+\gamma_k)(\hat{Q}_{k+1}-\hat{Q}_k)-(\gamma_k+\gamma_{k-1})(\hat{Q}_k-\hat{Q}_{k-1})]/[2(\Delta\eta)^2]$$

Analogous terms in the η and ζ directions are defined similarly.

Upper Bound of β

The criteria given by equations (5a) and (5b) fix the lower bound of β for obtaining converged numerical solutions. Howevereq, a large value of β makes the added pressure term in the continuity equation very small, which in turn causes the pseudo-compressible formulation to become very stiff [8]. Therefore, the upper bound of β depends on the particular numerical algorithm chosen. For example, if an explicit scheme is used, the stability condition associated with the pseudosound speed must be satisfied just as in the case of compressible flows.

The approximate-factorization algorithm used in the present study has a different feature to be considered. In factoring the finite-difference form of the governing equations to obtain equation (13), higher-order cross-differencing terms are added to the left-hand side of equation (8). The added terms consist of the product of $\hat{A}$ as follows:

$$\frac{h^2}{4}(J^{n+1})^2\delta_\xi\hat{A}_1{}^n\delta_\eta\hat{A}_2{}^n\Delta Q,$$
$$\frac{h^3}{8}(J^{n+1})^3\delta_\xi\hat{A}_1{}^n\delta_\eta\hat{A}_2{}^n\delta_\zeta\hat{A}_3{}^n\Delta Q,\quad ...etc. \tag{14a}$$

where

$$\Delta Q=Q^{n+1}-Q^n \tag{14b}$$

These added terms contaminate the momentum equations as well as the continuity equation, and therefore must be kept smaller than the original terms everywhere in the computational domain; that is,

$$O\left\{(\frac{h}{2}J)^2\delta_\xi\hat{A}_1\delta_\eta\hat{A}_2\right\}<O\left\{\frac{h}{2}J\delta_\xi\hat{A}_1\right\} \tag{15}$$

From the expression given by equation (9), this requirement leads to the following criterion for the upper bound of β:

$$\beta h<O(1) \tag{16}$$

If β is chosen to be larger than the above range, the accuracy of the numerical solution will deteriorate significantly and can even induce numerical instability.

IV. Computed Results

Numerical experiments are performed to verify both the present algorithm and the criteria for β which were based on a one-dimensional linear analysis. The magnitude of β is determined by the geometric and physical parameters such as the characteristic length of the body in the flow direction, Reynolds number, and the time-step size used for iteration. Also the influence of the β term on convergence rate and accuracy is investigated. As a measure of convergence, root-mean-square values of ΔQ (denoted by RMSDQ) in equation (13) are monitored. The accuracy of the solution can be tested by checking how accurately the divergence-free velocity field is attained. The first term of ΔQ in equation (13) can be regarded as a parameter showing how well the modified continuity equation (1f) is satisfied. The root-mean-square value of this quantity is denoted by RMSCO, which contains smoothing terms of the present algorithm. The true incompressibility is tested by using the root-mean-square value of (div u). In the following test problems, these quantities, namely, RMSDQ, RMSCO, and RMS(div u), will be shown to be functions of other parameters.

Flow through a Channel

The channel flow is perhaps the simplest internal flow test problem, where the pressure wave propagates between the inflow and outflow boundaries while the viscous effect spreads inward from two walls. The coordinate system used for this problem is shown in figure 1a, where velocity vectors for a converged solution are also shown. To obtain fully developed velocity profiles within a reasonable channel length, a partially developed boundary-layer profile is imposed at the inflow boundary which leaves a flat core region in the middle. In figure 1b, a converged velocity profile is compared with a fully developed velocity profile. In this experiment, the reference length and reference velocity are

$$x_{ref}=2h=channel\quad height$$
$$u_{ref}=u_{avg}$$

Tests are performed using the following three cases:

$Case 1.\ L=20, Re=1000, \Delta\tau=0.1: 0.75<\beta<10$

$Case 2.\ L=30, Re=1000, \Delta\tau=0.1: 1.19<\beta<10$

$Case 3.\ L=40, Re=1000, \Delta\tau=0.1: 1.69<\beta<10$

The Reynolds number and the time-step size are kept unchanged while the dimensionless channel length is varied from 20 to 40. This effectively changes the ratio of the time scales required for the pressure waves and the vorticity to map the entire flow field. For example, the time required for the pressure wave to make one round trip from the inlet to the exit boundary will be doubled when the channel length is increased from 20 to 40 while the vorticity spreads to the middle of the channel in about the same time. This requires a higher wave traveling speed in the algorithm. In the test cases, the minimum and the maximum value of β are estimated using equations (5a) and (16), respectively. In table 1, the number of iterations for one round-trip

by the pressure wave is tabulated for various values of β which include values outside the recommended range.

In figure 2, RMSDQ histories are shown for the above three cases. For all cases, $\beta = 0.1$ is much smaller than the minimum β required. For L=20, the iteration procedure becomes unstable after 340 steps, and for L=30 and L=40, the solution seems to be converging.

In figure 3, RMSDQ histories are plotted in terms of the number of round trips made by the pressure waves, N/N_1, between the inlet and exit boundary of the channel. In each case, runs with different β are plotted at the same interval of the iteration count; that is, in figure 3a, the number of iterations using $\beta = 1$ is approximately 3 times greater than the number using $\beta = 5$ for the pressure wave to reach a same distance. These plots show that most variations in RMSDQ take place before N/N_1 reaches 1. By the time waves complete two round trips, that is $N/N_1 = 2$, RMSDQ values are fairly well converged. Using $\beta = 0.1$, the number of iterations to reach $N/N_1 = 1$ is 4196 for $L = 20$ and becomes 8391 for $L = 40$. These requirements are not acceptable for practical applications even if the solutions converge. Moreover, the accuracy deteriorates, as will be shown next. Therefore, the computation is not continued to reach $N/N_1 = 2$ for *case* 3.

In figure 4, RMS(div u) values are plotted to check the accuracy of the converged solutions. When the value of β is out of the range specified for the test cases, the accuracy of the solution measured by the incompressibility deviates from that expected by the truncation error analysis of the differencing scheme. For example, when β is increased to 50, the incompressibility is not very well satisfied. Using $\beta = 0.1$, the accuracy becomes very poor. Since the Mach number based on the pseudosound speed in equation (2) becomes very large in this case, the pseudocompressible effect becomes significant. This causes the vorticity and the pressure wave to interact improperly, failing to produce an incompressible effect. This aspect will be illustrated further in figure 6.

In figure 5, RMS(div u) values are plotted in terms of N/N_1. These plots also show that about two round trips of the pressure waves are required to obtain converged solutions. These experiments show that a lower value of β within the required range reduces the approximate-factorization error at the expense of increased iteration.

In figure 6, RMSCO and RMS(div u) are compared for *case* 2. For $\beta = 0.1$, which is much smaller than required, RMSCO is converging which indicates that the modified continuity equation (1f), including smoothing terms, is reasonably well satisfied. However, RMS(div u) deviates from RMSCO considerably because of the pseudocompressible effect of the present formulation. For $\beta = 1$, which is slightly smaller than the lower bound, RMS(div u) is converging slowly, even though its magnitude is still substantially different from that of RMSCO. For $\beta = 2$, which is within the recommended range, RMSCO and RMS(div u) are both converging satisfactorily.

In figure 7, the RMSCO history for all cases is shown.

Flow through a Turn-Around Duct

To test internal flows further, an annular duct with a 180° bend is chosen. This configuration is similar to the turn-around duct of the hot-gas manifold in the Space Shuttle main engine (SSME). In figure 8, the geometry and a laminar solution at Re=1,000 are shown, which reveals the formation of a large separated bubble after the 180° bend. For this geometry, the streamwise length normalized by the duct width is 20. Using equation (5a) and (16), the values of β are obtained for $Re = 1,000$ and 100 with $\Delta\tau = 0.1$

$$0.17 << \beta < 10. \quad for \quad Re = 1,000$$

$$2.24 << \beta < 10. \quad for \quad Re = 100$$

The test problems presented here were treated using a 51 x 17 x 21 mesh for half-duct formulation.

In figures 9a and 9b, the influence of β on the convergence and the accuracy is shown for $Re = 1,000$. As a measure of incompressibility and the convergence, the RMSCO values are shown in figure 9a. As the solution converges to the steady state, this quantity must approach zero to satisfy the continuity equation. Another important quantity to observe is the maximum total pressure at any point in the computational domain. Here, the total pressure is defined by the following expression:

$$C_{po} = \frac{p_o - p_{o1}}{p_{o1}}$$

where

$$p_o = p + \frac{1}{2}(u^2 + v^2 + w^2)$$

and p_{o1} is the total pressure at the inlet. The dependence of the maximum total pressure on the magnitude of β is shown in figure 9b. This experiment clearly shows that if β is chosen either too large or too small, the solution is not converging. Moreover, if the value of β is too large, the approximate-factorization scheme is contaminated to the point that the incompressibility is not satisfied.

A similar experiment is done for the case with $Re = 100$, and the results are shown in figures 10a and 10b.

External-Flow Test Problem

To represent an external flow, the flow past a circular cylinder at a $Re = 40$ was chosen. For external flows, in which the computational domain extends a large distance from the body, the pressure waves originating from the body surface propagate into

the far-field. Therefore, to obtain the near-field solution only, the distance traveled by the waves and the spreading of the vorticity can be approximately the same in magnitude. In the present case, if the viscous region is taken to be approximately two diameters away from the body, equation (5a) leads to the following range for β using $\Delta\tau = 0.1$:

$$0.1 << \beta < 10$$

This indicates that the magnitude of β is less restrictive for external flows in general.

In figures 11a and 11b, the stream-function contours and the pressure coefficient on the surface are shown for a steady-state solution. This solution agrees very well with that of Mehta who used a stream function and vorticity formulation in two dimensions (personal communication from U. B. Mehta, 1983). In figure 12, where the history of the pressure drag is shown for an impulsively started circular cylinder at $Re = 40$, four different values of β were compared with the time-accurate solution of Mehta. In all cases, the values of β are selected within the suggested range above, and the solutions converge quite rapidly.

The computing time required for the present experiments was 1.1 x 10^{-4} sec per mesh point per time-step on the Cray X-MP computer at NASA Ames Research Center.

V. Concluding Remarks

This paper presents salient features of the computational method developed for a three-dimensional, incompressible, Navier-Stokes code (INS3D) [11]. INS3D has been applied to various geometrically complex flows, including a major application in analyzing the complex flow field in the Space Shuttle main engine power head. The present study clarifies physical and numerical characteristics of the pseudocompressible approach in simulating incompressible flows. The present algorithm has been shown to be very robust and accurate if the selection of β is made according to the guidelines presented here. For time-accurate solutions and also for improvement in the convergence rate, an iteration algorithm utilizing equation (1g) is being investigated. The effectiveness of this method will be published in a future report.

References

1. Mehta, U. B.: Dynamic Stall of an Oscillating Airfoil, Paper No.23, AGARD Conference Proceedings No. 227, Ottawa, Canada, Sept. 1977.

2. Shang, J. S.; Buning, P. G.; Hankey, W. L.; and Wirth, M. C.: Performance of a Vectorized Three-Dimensional Navier-Stokes Code on the Cray-1 Computer, AIAA J., vol. 18, no. 9, Sept. 1980, pp. 1073-1079.

3. Hung, C. M.; and Kordulla, W.: A Time-Split Finite-Volume Algorithm for Three-Dimensional Flow-Field Simulation, AIAA Paper 83-1957, Danvers, Mass., 1983.

4. Pulliam, T. H.; and Steger, J. L.: Implicit Finite-Difference Simulations of Three-Dimensional Compressible Flow, AIAA J., vol. 18, no. 2, 1980, pp. 159-167.

5. Briley, W. R.; and McDonald, H.: Solution of the Three-Dimensional Compressible Navier- Stokes Equations by an Implicit Technique, Proceedings of Fourth International Conference on Numerical Methods in Fluid Dynamics, Lecture Note in Physics, vol. 35, Springer-Verlag, New York, 1975, pp. 105-110.

6. Harlow, F. H.; and Welch, J. E.: Numerical Calculation of Time-Dependent Viscous Incompressible Flow with Free Surface, Phys. of Fluids, vol. 8, no. 12, Dec. 1965, pp. 2182-2189.

7. Chorin, A. J.: A Numerical Method for Solving Incompressible Viscous Flow Problems, J. Comput. Phys., vol. 2, 1967, pp. 12-26.

8. Steger, J. L.; and Kutler, P.: Implicit Finite-Difference Procedures for the Computation of Vortex Wakes, AIAA J., vol. 15, no. 4, Apr. 1977, pp. 581-590.

9. Beam, R. M.; and Warming, R. F.: An Implicit Finite-Difference Algorithm for Hyperbolic Systems in Conservation-Law Form, J. Comput. Phys., vol. 22, Sept. 1976, pp. 87-110.

10. Chakravarthy, S. R.: Numerical Simulation of Laminar Incompressible Flow within Liquid Filled Shells, Report ARBRL-CR-00491, U.S. Army Ballistics Research Laboratory, Aberdeen Proving Ground, Md., Nov. 1982.

11. Kwak, D.; Chang, J. L. C.; Shanks, S. P.; and Chakravarthy, S.: An Incompressible Navier-Stokes Flow Solver in Three-Dimensional Curvilinear Coordinate Systems Using Primitive Variables, AIAA Paper 84-253, Reno, Nev., 1984.

12. Chang, J. L. C.; and Kwak, D.: On the Method of Pseudo Compressibility for Numerically Solving Incompressible Flows, AIAA Paper 84-252, Reno, Nev., 1984.

Table 1: Number of iterations required for one round-trip by pressure waves between in- and out-flow boundary of a channel: Re = 1000 and $\Delta\tau$ = 0.1

β		0.1	1	2	5	10	50
N_1	L = 20	4196	566	347	196	133	58
	L = 30	6293	849	520	294	199	86
	L = 40	8391	1132	693	392	266	115

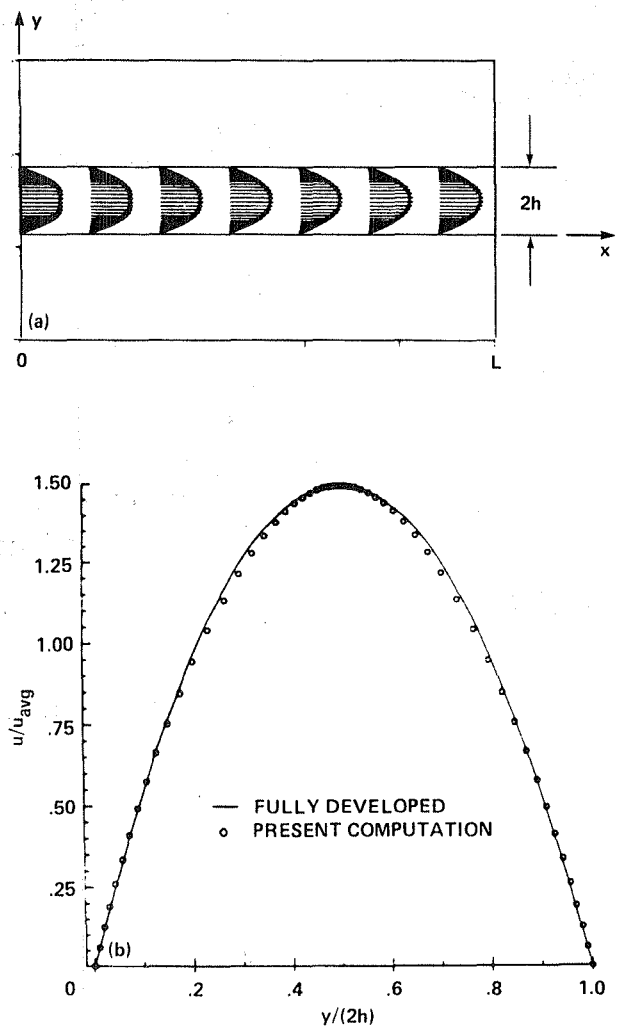

Figure 1.– Developing laminar channel flow at Re = 1,000 (Re based on channel width and average velocity). (a) Velocity vector. (b) Fully developed velocity profile.

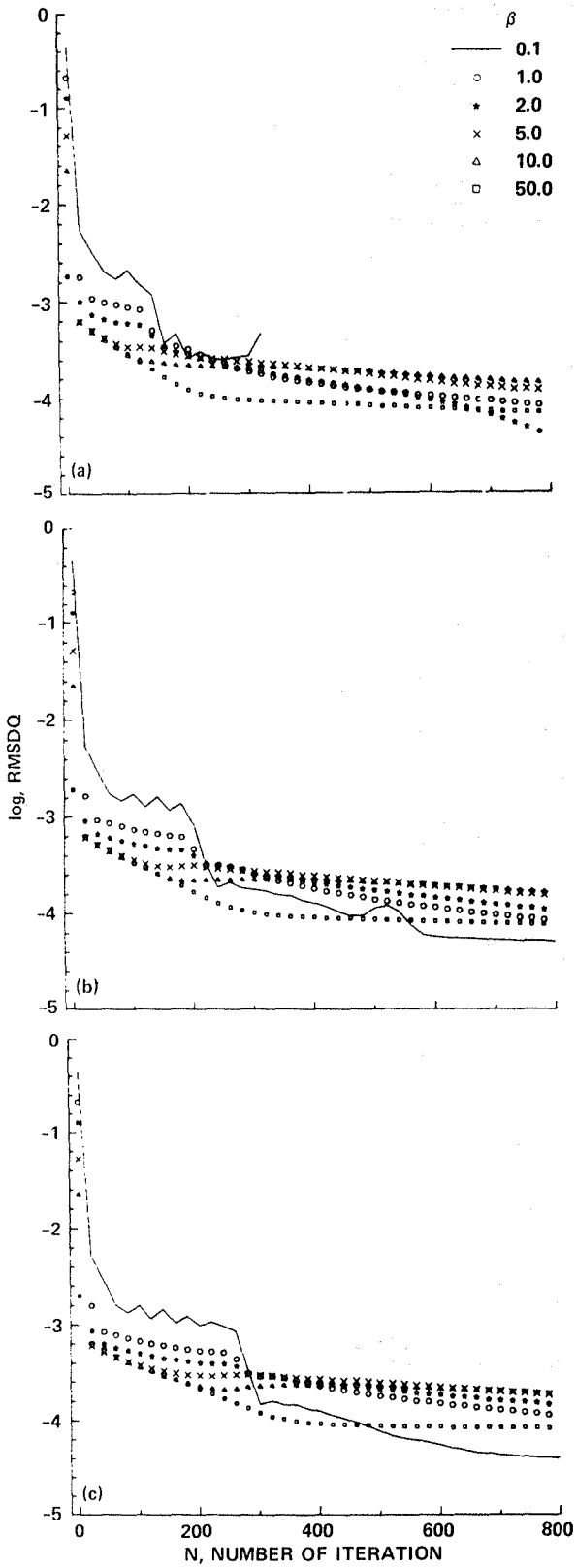

Figure 2.– RMSDQ history for channel flow at Re = 1,000 and $\Delta\tau$ = 0.1. (a) L = 20. (b) L = 30. (c) L = 40.

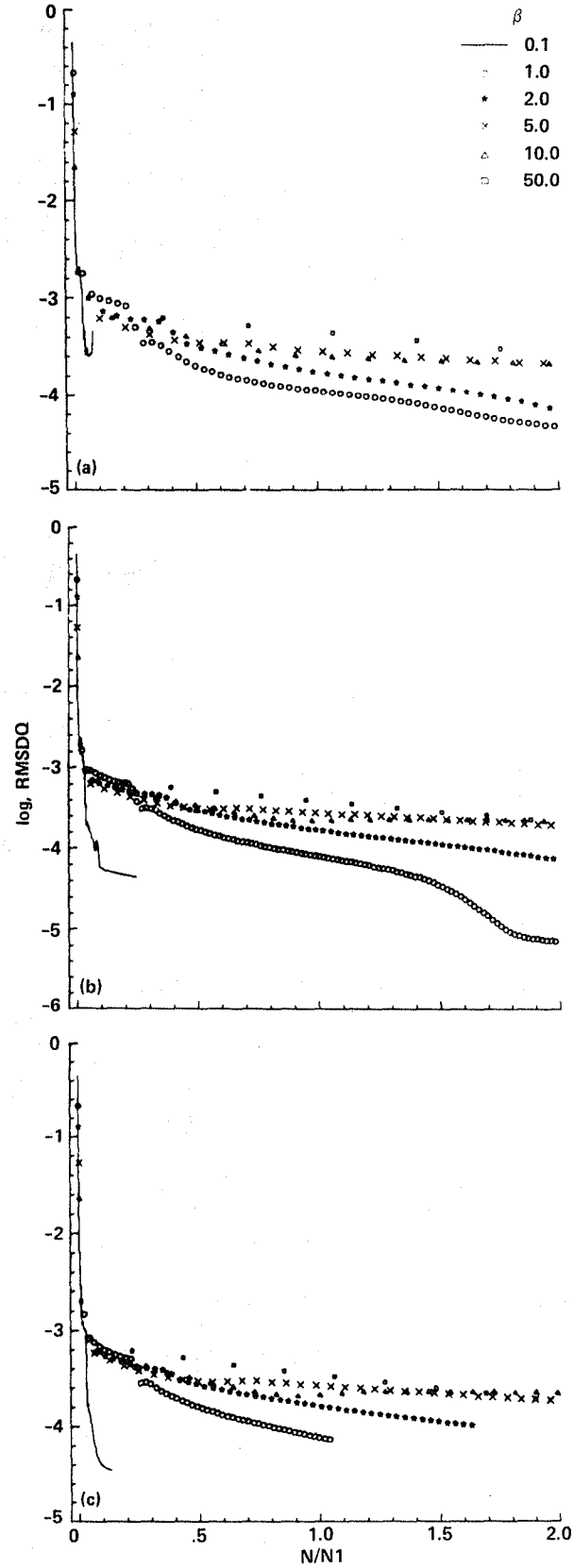

Figure 3.– RMSDQ vs number of roundtrips made by pressure waves between inflow and outflow boundary of a channel Re = 1,000 and $\Delta\tau$ = 0.1. (a) L = 20. (b) L - 30. (c) L = 40.

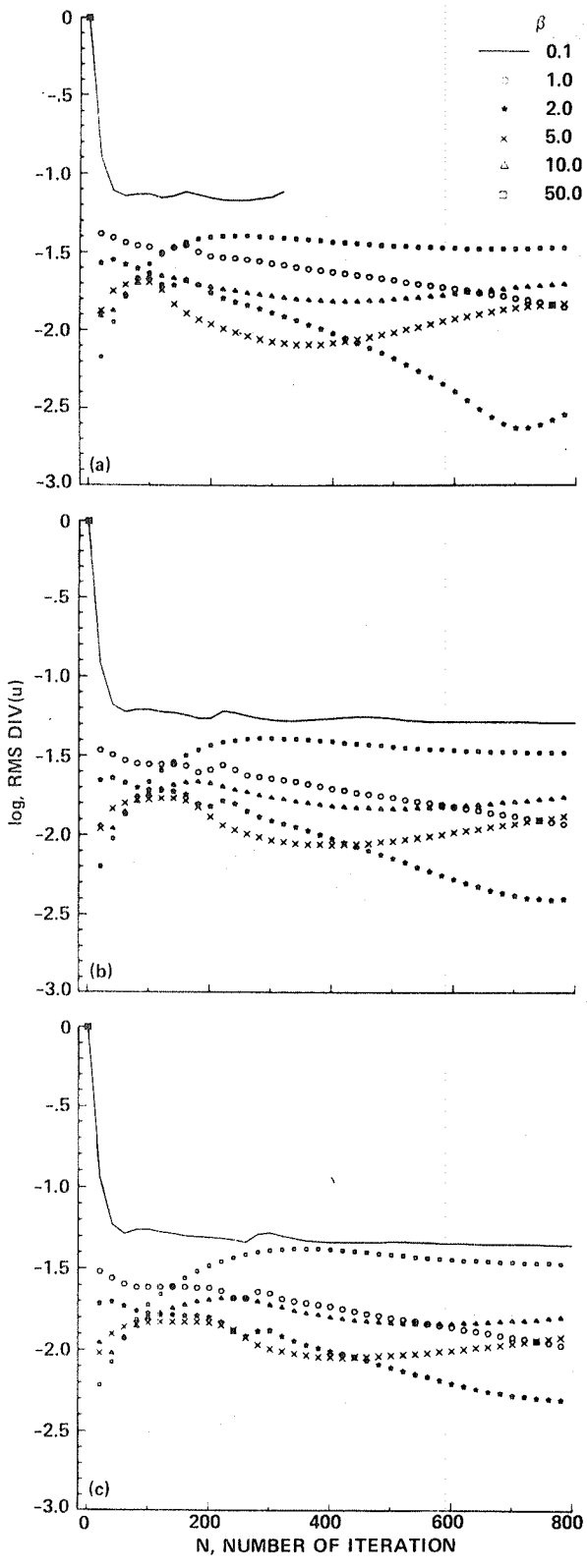

Figure 4.– RMS(div u) history for channel flow at Re = 1,000 and $\Delta\tau$ = 0.1. (a) L = 20. (b) L = 30. (c) L = 40.

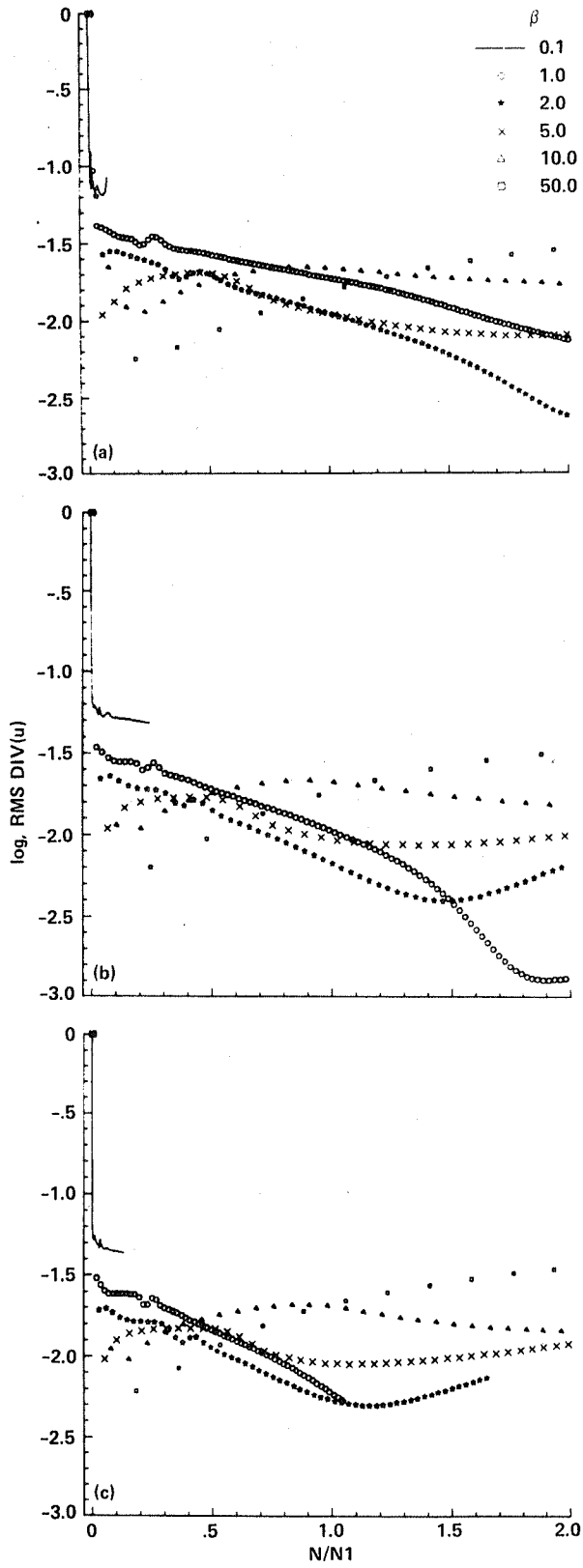

Figure 5.– RMS(div u) vs number of roundtrips made by pressure waves between inflow and outflow boundary of a channel Re = 1,000 and $\Delta\tau$ = 0.1. (a) L = 30. (b) L = 30. (c) L - 40.

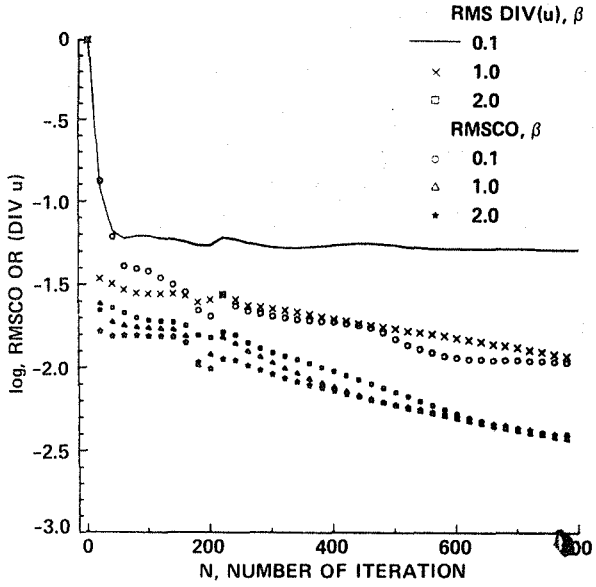

Figure 6.– Comparison of RMSCO and RMS(div u) history for channel flow: Re = 1,000, $\Delta\tau$ = 0.1, L = 30.

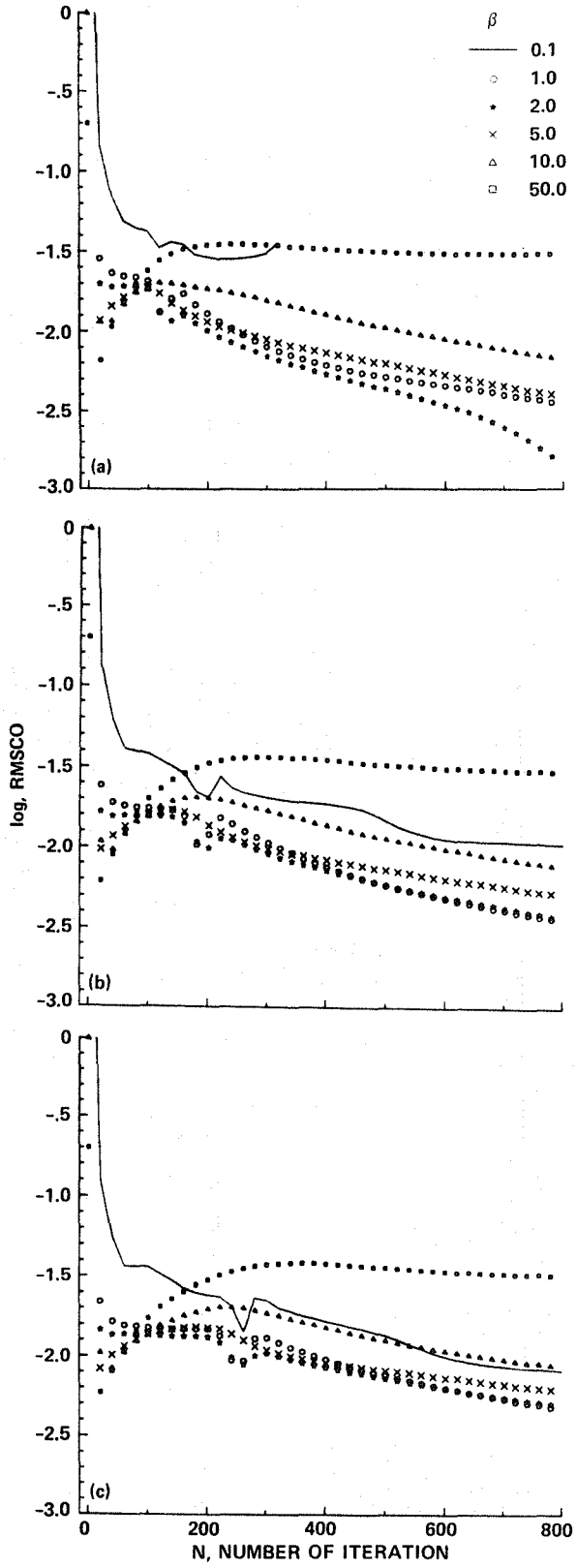

Figure 7.– RMSCO history for channel flow at Re = 1,000 and $\Delta\tau$ = 0.1. (a) L = 20. (b) L = 30. (c) L = 40.

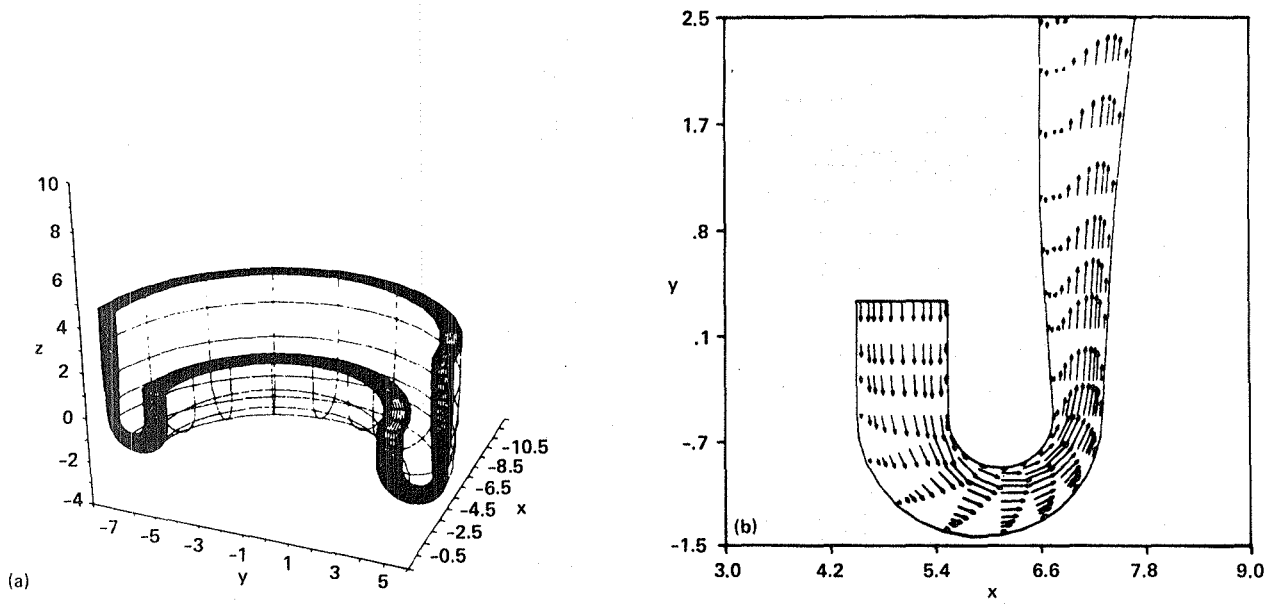

Figure 8.– Flow through a turn-around duct. (a) Three-dimensional grid. (b) Typical flow pattern with separation (Re = 1,000).

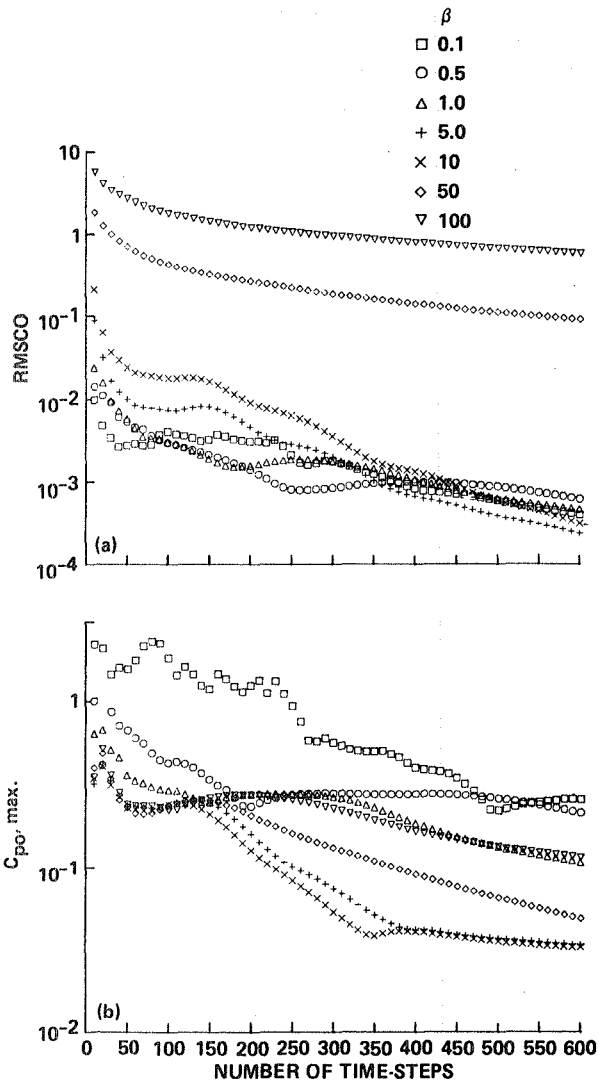

Figure 9.– Influence of β on incompressibility and convergence for turn-around duct at Re = 1,000.

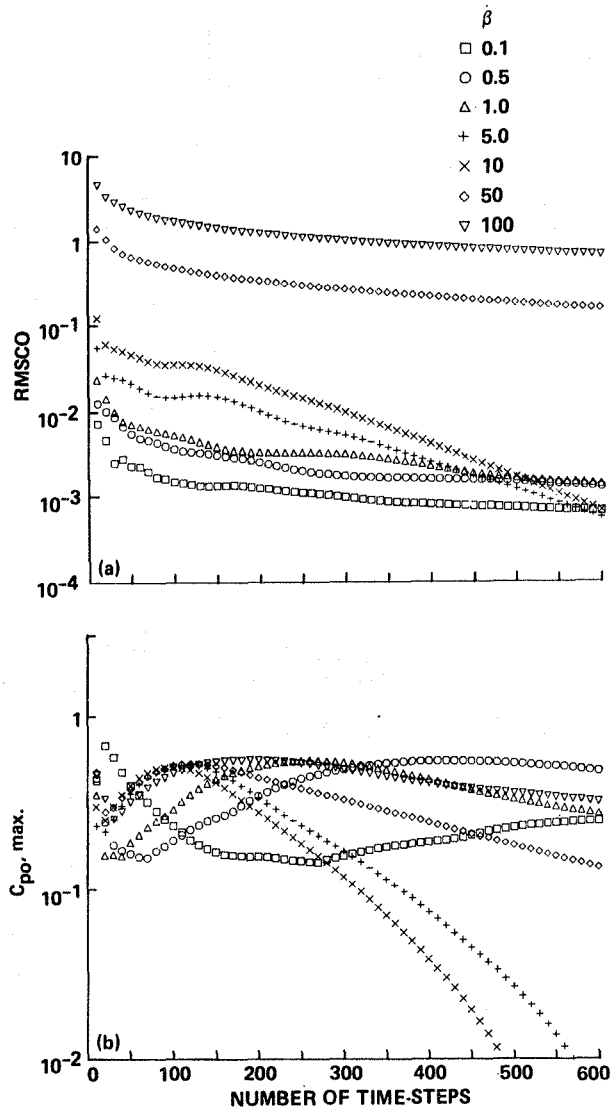

Figure 10.– Influnce of β on incompressibility and convergence for turn-around duct at Re = 1,000.

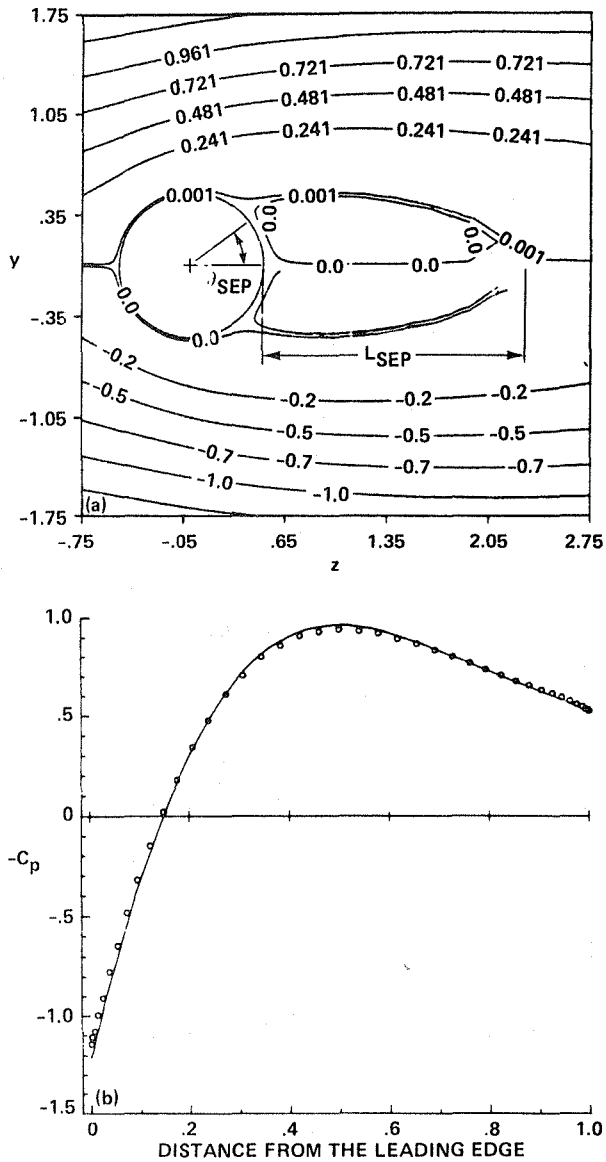

Figure 11.– Steady-state solution for flow over a circular cylinder at Re = 40. (a) Stream-function contours. (b) Pressure coefficient on the cylinder.

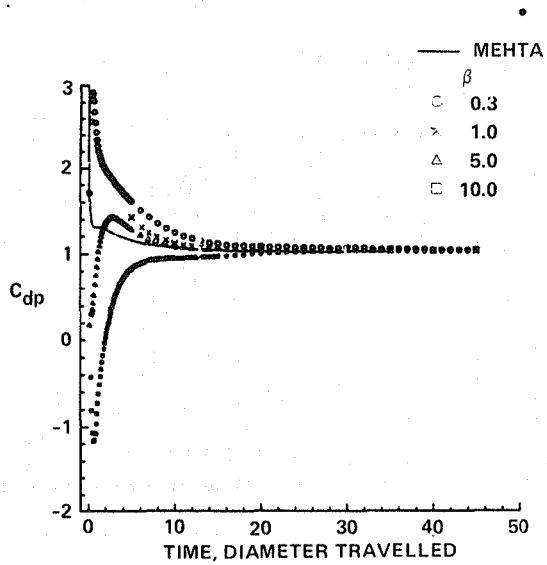

Figure 12.– Influence of β on convergence for flow over a circular cylinder at Re = 40.

1. Report No.	2. Government Accession No.	3. Recipient's Catalog No.
NASA TM-85958		

4. Title and Subtitle	5. Report Date
A COMPUTATIONAL METHOD FOR VISCOUS INCOMPRESSIBLE FLOWS	May 1984
	6. Performing Organization Code
7. Author(s)	8. Performing Organization Report No.
Dochan Kwak and James L. C. Chang (Rocketdyne Division, Rockwell International, Canoga Park, CA)	A-9748
	10. Work Unit No.
9. Performing Organization Name and Address	T-6458
Ames Research Center Moffett Field, CA 94035	11. Contract or Grant No.
	13. Type of Report and Period Covered
12. Sponsoring Agency Name and Address	Technical Memorandum
National Aeronautics and Space Administration Washington, DC 20546	14. Sponsoring Agency Code 505-31-01

15. Supplementary Notes

Point of Contact: Dochan Kwak, Ames Research Center, M.S. 202A-14, Moffett Field, CA 94035 (415) 965-6743 or FTS 448-6743

16. Abstract

An implicit, finite-difference procedure for numerically solving viscous incompressible flows is presented. The pressure-field solution is based on the pseudocompressibility method in which a time-derivative pressure term is introduced into the mass-conservation equation to form a set of hyperbolic equations. The pressure-wave propagation and the spreading of the viscous effect is investigated using simple test problems. Computed results for external and internal flows are presented to verify the present method which has proved to be very robust in simulating incompressible flows.

17. Key Words (Suggested by Author(s))	18. Distribution Statement
Viscous incompressible flow	Unlimited Subject Category - 02

19. Security Classif. (of this report)	20. Security Classif. (of this page)	21. No. of Pages	22. Price*
Unclassified	Unclassified	15	A02

*For sale by the National Technical Information Service, Springfield, Virginia 22161

End of Document